Available online at www.sciencedirect.com
SCIENCE DIRECT
Journal of Solid State Chemistry 179 (2006) 1161–1170
JOURNAL OF SOLID STATE CHEMISTRY
www.elsevier.com/locate/jssc

Preparation, phase transformation and photocatalytic activities of cerium-doped mesoporous titania nanoparticles

Jiangrong Xiao[a], Tianyou Peng[a,*], Ran Li[a], Zhenghe Peng[a], Chunhua Yan[b]

[a]*Department of Chemistry, Centre of Nanoscience and Nanotechnology Research, Wuhan University, Wuhan 430072, China*
[b]*State Key Laboratory of Rare Earth Materials Chemistry and Applications, Peking University, Beijing 100871, China*

Received 28 October 2005; received in revised form 30 December 2005; accepted 3 January 2006
Available online 23 February 2006

Abstract

Cerium-doped mesoporous TiO_2 nanoparticles with high surface area and thermal stable anatase wall were synthesized via hydrothermal process in a cetyltrimethylammonium bromide (CTAB)/$Ti(SO_4)_2$/$Ce(NO_3)_4$/H_2O system. The obtained materials were characterized by XRD, FESEM, HRTEM, FTIR spectroscopy, nitrogen adsorption and DRS spectra. Experimental results indicated that the doping of cerium not only increased the surface area of mesoporous TiO_2 nanoparticles, but also inhibited the mesopores collapse and the anatase-to-rutile phase transformation. Moreover, the undoped, doped anatase mesoporous nanoparticles exhibit higher photocatalytic activity than commercial photocatalyst (Degussa, P25), but the maximum photodegradation rate corresponds to the undoped mesoporous TiO_2 nanoparticles. The lower photocatalytic activities of cerium-doped samples compared with undoped one may be ascribed to that the doped cerium partially blocks titania's surface sites available for the photodegradation and absorption of Rhodamine B (RB).

Keywords: Cerium doped; Mesoporous materials; Titania; Nanoparticles; Anatase

1. Introduction

In the past decades, there are numerous researches focused on the synthesis of titania with sizes ranging from nanoscale to micrometer scale and various microstructures for the photocatalysis and photoelectrode materials [1,2]. Among the three nature crystalline phases of titania: brookite, anatase and rutile, anatase is believed to possess enhanced photocatalytic and photoelectrochemical conversion performances probably because of its open structure compared with that of rutile [3,4]. Since anatase is a metastable titania polymorph, it tends to transform into the rutile upon calcination, along with decreasing the surface area, resulting in a loss of photocatalytic activity. In order to overcome these difficulties, there are two main modifications, which frequently lead to a considerable improvement of their photocatalytic performances. One is careful control of the microstructures (such as the surface area, crystal phase, the crystallite size and the morphology of the individual particle, etc.) [5,6]. The other is incorporation of metals like platinum and nickel to the photocatalysts, which can also result in an increase of the degradation efficiencies most probably because of the stabilization of the photogenerated charge carriers [7]. Similarly, doping of transition metal ions on the titania can also significantly enhance the quantum efficiency, either by expanding the light absorption range or by improving the redox potential of the photogenerated radicals [3,8–10].

For the microstructure controlling, mesoporous TiO_2 has attracted much attention due to its high surface-to-volume ratio and offers more active sites, which are of great importance in photocatalysis and solar energy conversion [7–15]. Up till now, surfactants [11–13], triblock copolymer [14], and some nonsurfactant organic compounds [15] have been successfully used to prepare mesoporous TiO_2. Generally, the precipitates derived from sol–gel and/or co-precipitate processes through self-assembly mechanics are amorphous in nature [16], the photoactivities of those obtained amorphous or semicrystalline

*Corresponding author. Fax: +86 27 6875 4067.
E-mail address: typeng@whu.edu.cn (T. Peng).

0022-4596/$ - see front matter © 2006 Elsevier Inc. All rights reserved.
doi:10.1016/j.jssc.2006.01.008

TiO_2 are not high enough for industrial purposes [17,18]. Calcination at elevated temperature may not be beneficial for improvement of the photocatalytic activity as it results in collapse of the mesoporous framework and loss of surface area due to the crystallization and growth of TiO_2 nanocrystallites [19]. Since the anatase has a far higher photocatalytic activity than amorphous and rutile TiO_2, therefore, there is still a challenge to synthesize mesoporous TiO_2 containing high crystallinity anatase wall and large surface area [20,21]. On the other hand, numerous approaches have been conducted to extend the light absorption range of TiO_2 and to improve its photoactivity by modifying its surface properties, composition, etc. [3,22–26]. It is usual to add other atoms to titania in order to improve TiO_2 properties such as anatase phase and mesostructure stability, specific photoelectrochemical and catalytic performances. Doping with transition metal ions has also been proven to be a potential route for the improvement of photoactivity of TiO_2 [24–26]. Lanthanide ions are known for their ability to form complexes with various Lewis bases (e.g., amines, aldehydes, alcohols, thiols, etc.) in the interaction of these functional groups with the *f*-orbitals of lanthanides [9,27–31]. Frindell et al. [30] have proved that the europium ions are located in amorphous titania regions near the interface between the anatase nanocrystallites, and the well-ordered mesostructure is preserved. Zhang and Pinnavaia [31] have reported that the incorporation of 1–5 mol% cerium or lanthanum ions dramatically improved alumina's thermal stability without altering the mesopore size. Therefore, it is expected that incorporation of lanthanide ions on TiO_2 could not only provide a means to concentrate the organic pollutants at the semiconductor surface, but also stabilize the mesostructure and provide high surface area, and therefore enhance the photocatalytic activity of TiO_2 [20].

CeO_2 is frequently incorporated to catalysts due to its considerable performance for the catalytic combustion of hydrocarbons [32]. It has been reported that CeO_2 has the property of stabilizing the active phase and inhibiting the thermal loss of the catalyst surface area and the catalytic activity [32–34]. However, there are only a few reports on the photocatalytic activity of cerium-doped materials [29,35,36]. In our previous publications [37,38], the syntheses and characterizations of TiO_2 nanoparticle with anatase mesostructures have been reported. This kind of materials combined with the properties of nanoscale powders and mesoporous materials, which would have an advantage in relate to photocatalytic and photoelectrochemical performances. Herein, cerium-doped TiO_2 nanoparticles with anatase mesostructures were fabricated via hydrothermal process by using cetyltrimethylammonium bromide (CTAB) as a directing and pore-forming agent. The effect of cerium doping on the phase transformation, photocatalytic activity for the mineralization of Rhodamine B (RB) in air was also investigated.

2. Experimental

2.1. Preparation of Ce-doped mesoporous TiO_2 nanoparticles

All chemical reagents used in the present experiments were obtained from commercial sources and used without further purification. $Ti(SO_4)_2$ (CP, Shanghai Chemical Agent Factory, China). $Ce(NO_3)_4$ (Ar, Shanghai Henke Rared-earth Refined Chemical and Technological Co., China). CTAB (Ar, Shanghai Sanpu Chemical and Technological Ltd., China).

In a typical process, $Ti(SO_4)_2$ was dissolved into 7.0 mL distilled water. And subsequently $Ce(NO_3)_4$ was added to the $Ti(SO_4)_2$ aqueous solution. The obtained solution was added into CTAB solution under stirring. The molar ratio of $Ti(SO_4)_2$:$Ce(NO_3)_4$:CTAB:H_2O is $(1-x)$:x:0.12:100 ($x = 0, 0.01$ or 0.05), the pH value is ca. 0.6. After stirring for 30 min, the mixture was aged at room temperature for 12 h, and then transferred into an autoclave at 100 °C for hydrothermal treatment. After 72 h, the resulting powders were cooled to room temperature, then recovered by centrifugation, washed with water and ethanol, and then dried at 120 °C overnight.

In order to remove organic materials, ion-exchange treatment was performed by mixing the obtained powders with a water and ethanol (molar ratio 1:1) solution of sodium chloride under stirring at 40 °C for 5 h. The resulting solids were washed with water and ethanol, then dried at 120 °C overnight. To improve crystallinity of obtained products, the as-synthesized samples were calcined at 300, 500, 800, 900 °C for 2 h with a heating rate of 2 °C min^{-1}, respectively.

2.2. Characterization of doped mesoporous TiO_2 nanoparticles

Field emission scanning electron microscopy (FESEM) images were observed on a JSM-7400F electron microscope (Japan Electronics, Japan). Transmission electron microscopy (TEM) images were obtained on a JEM-100CX II and LaB_6 JEM-2010(HT)-FEF (HRTEM) electron microscope (Japan Electronics, Japan). X-ray diffraction (XRD) patterns were performed on D_8-advance X-ray diffractometer (Bruker, Germany) using Cu$K\alpha$ as radiation. The nitrogen adsorption–desorption isotherms at 77 K were measured on a Micromeritics ASAP 2010 system (Micromeritics, America) after samples were degassed at 120 °C. FTIR spectra were recorded on an FTIR-8201PC spectrometer (Nicolet, America). UV-Vis diffuse reflectance spectra (DRS) were performed with a Cary 5000 UV-Vis-NIR spectrophotometer (Varian, America) equipped with an integrating sphere.

2.3. Photocatalytic activity

The photocatalytic experiments on the mesoporous TiO_2 nanoparticles for the photo-degradation of RB in air were

performed at room temperature. The UV source was a 300 W Hg lamp (100 mm long) with a maximum emission at approximately 365 nm, which was surrounded by a circulating water jacket (Pyrex) to cool the lamp. In a typical process, the aqueous RB/TiO_2 suspension was prepared by addition of TiO_2 (50 mg) to a 50 mL aqueous solution containing RB dye ($c_0 = 1.0 \times 10^{-5}$ M, pH 6.0). All runs were conducted at ambient pressure and room temperature. The distance between the Hg lamp and the reactor was 30 cm for each experiment. The suspension was magnetic stirred before and during illumination. The suspension was mixed for 15 min in the dark (for the adsorption of dye onto the surface of photocatalyst) and then the reaction mixture was exposed to the UV light. After irradiation and removal of the TiO_2 particles by centrifugation, the residual RB was analyzed using a Shimadzu UV-240 spectrophotometer. For comparison, commercial photocatalyst Degussa P25 was also been conducted under an identical experimental condition.

3. Results

3.1. X-ray diffraction analysis

The low-angle XRD patterns of the 1 mol% cerium-doped samples are shown in Fig. 1. Except for the sample calcined at 800 °C, all patterns are similar and exhibit a single diffraction peak corresponding to *d*-spacings of 5.54 5.48, 5.42 and 5.25 nm for samples as-synthesized, calcined at 300, 500 and 800 °C, respectively. This single strong diffraction peak in the low-angle region indicated the presence of mesostructure in samples [21,37,38]. Mesostructures with more or less regular in diameter channel packed at random often display a single peak in low-angle XRD [21,37]. Upon calcinations, the considerable broadening and reducing in the intensity of diffraction peak, as well as the shifting of *d*-spacing to lower distances can be attributed to the partial collapse and/or shrinkage of the mesostructure upon calcination. A single broad peak is observed on low-angle XRD pattern even for the sample calcined at 500 °C, implying the considerably high thermal stability of the mesoporous framework in the obtained samples. Wang et al. [21] had reported that the amorphous TiO_2 gel derived from sol–gel process can be crystallized into anatase and stabilized mesoporous structure TiO_2 by a post-hydrothermal treatment. Moreover, rare-earth ions have been used by other groups as stabilizing agents to slow down condensation during the synthesis of mesoporous materials [30,31,39]. While slower condensation between individual TiO_2 precursor could lead to the well-crystallized anatase mesostructure. Therefore, we think that the hydrothermal treatment is also beneficial for crystallizing porous wall into the anatase and effectively increasing its thermal stability in the present work, thus preventing the mesopores from collapse upon calcination.

The high-angle XRD results for the as-synthesized samples reveal the coexistence of TiO_2-anatase (JCPDS, No. 21-1272, Fig. 2a, undoped sample) and CeO_2-cerianite (JCPDS, No. 43-1002, Fig. 2b and c, cerium-doped samples). Upon increasing cerium-doped amount, the diffraction peaks of anatase phase (undoped TiO_2 sample, Fig. 2a) became broadening and reducing in intensity, while those of cerianite phase (Fig. 2b and c) became stronger, implying that the cerium doping results in decrease of the nanocrystallite size. It may be ascribed to the segregation of the dopant cations at the grain boundary, and preventing the growth of nanocrystallite in the nanoparticles. Also, the diffraction peaks (Fig. 3a–d) show that the anatase and cerianite phase in 1 mol%

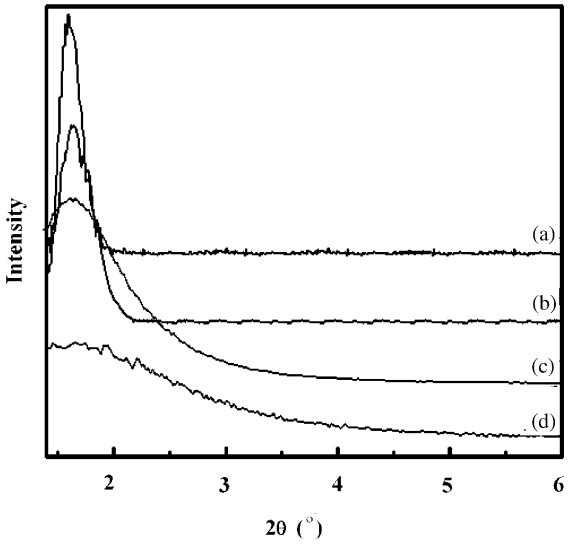

Fig. 1. Low-angle X-ray diffraction (XRD) patterns of the 1 mol% cerium-doped TiO_2: (a) as-synthesized, and calcined at (b) 300 °C, (c) 500 °C, (d) 800 °C.

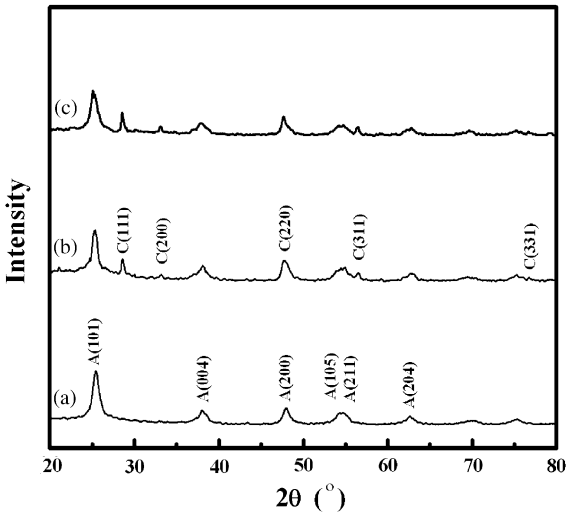

Fig. 2. High-angle X-ray diffraction (XRD) patterns of the as-synthesized: (a) undoped, (b) 1 mol% cerium, and (c) 5 mol% cerium-doped TiO_2 (A. anatase; C. cerianite).

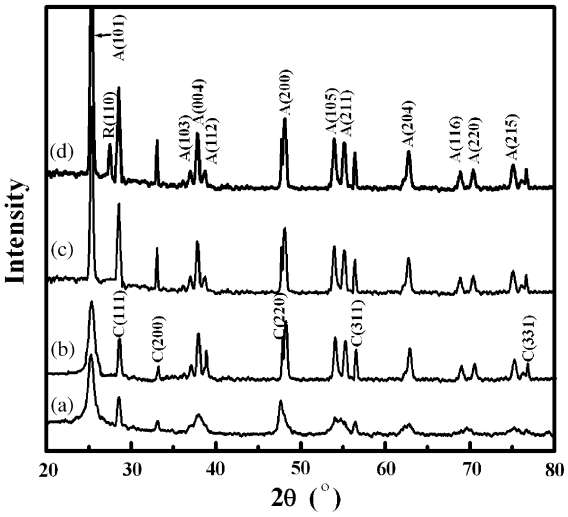

Fig. 3. High-angle X-ray diffraction (XRD) patterns of the 1 mol% cerium-doped TiO_2 calcined at: (a) 300 °C, (b) 500 °C, (c) 800 °C, and (d) 900 °C. (A. anatase; C. cerianite).

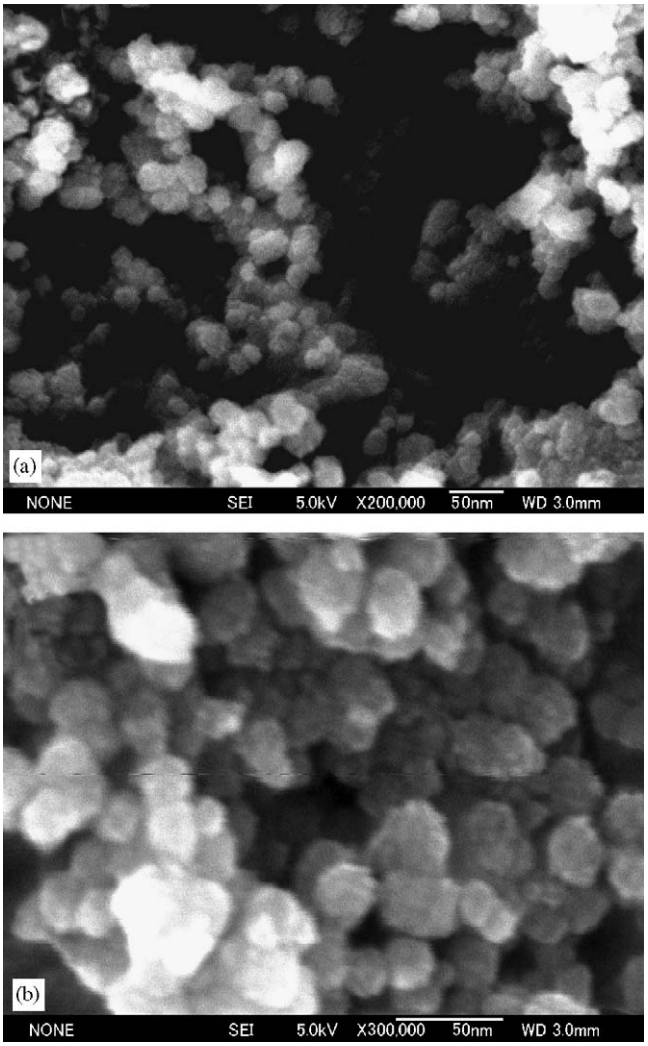

Fig. 4. FESEM images of 1 mol% cerium-doped samples: (a) as-synthesized and (b) calcined at 300 °C.

cerium-doped TiO_2 powders became sharper and stronger upon calcination. As indicated in Fig. 3d, even calcined at 900 °C for 2 h, the XRD pattern of the doped sample show that the main crystal phase of titania is still anatase with some smaller peaks related to the rutile, this high thermal stability of anatase is different from that the anatase-to-rutile transformation starts as early as 500–700 °C in the case of pure TiO_2 in the previous literatures [9,27–30]. Furthermore, no solid solution was identified since no significant peak shift of above-mentioned diffraction peaks was observed, it is consistent with previous report [34]. The high stability of the anatase phase may be attributed to the small crystallite size, mesostructures of inorganic domains and the formation of Ti–O–Ce bonds, which will be discussed below.

3.2. Microstructures analysis

Fig. 4 shows the FESEM images of the 1 mol% cerium-doped samples as-prepared and calcined at 300 °C. As can be seen, the as-synthesized sample has a relative uniform particle diameter in the range of 15–37 nm with mean particle size of 25 nm. After calcinations at 300 °C, the sample has particle size in the range of 14–35 nm with mean particle size of 22 nm. The HRTEM images of the obtained samples in Fig. 5 show the more detail microstructure of the nanoparticles. Mesoporous structure without long-range order can be clearly observed, which coincides with the single diffraction peak in the low-angle XRD patterns (Fig. 1). The morphologies of mesopores and nanoparticles are not changed significantly upon heating to 300 °C, indicating that reconstruction and/or collapse do not occur drastically upon calcination, although it can be observed that some particles have been cracked from the image of the sample calcined at 300 °C (Fig. 5c). The HRTEM image of the as-synthesized mesoporous sample (Fig. 5b) clearly shows that the anatase phase has already formed in the mesoporous wall. The inserted electron diffraction patterns in Fig. 5a also indicate that the crystallinity of anatase and cerianite phase in the mesoporous wall is very high, which is consistent with XRD analysis results of the doped samples (Fig. 2b). As can be seen from Fig. 5, the pore size and the wall thickness of the as-synthesized and calcined mesoporous TiO_2 nanoparticles are estimated to be 1.7–4.0 and 1.6–5.0 nm, respectively. In previous work with PEO-based surfactants, Yang et al. [14] found that these crystalline domains were embedded in the mostly amorphous TiO_2 matrix. Cabrera et al. had also reported 3 nm anatase located in the mesoporous walls of a wormlike material [40]. However, the mesoporous wall of as-synthesized samples basically composed of nanocrystalline with limited amount of amorphous TiO_2 matrix, implying that the hydrothermal treatment can efficiently crystallize the inorganic walls into anatase and cerianite phase while preserving the mesostrucutre.

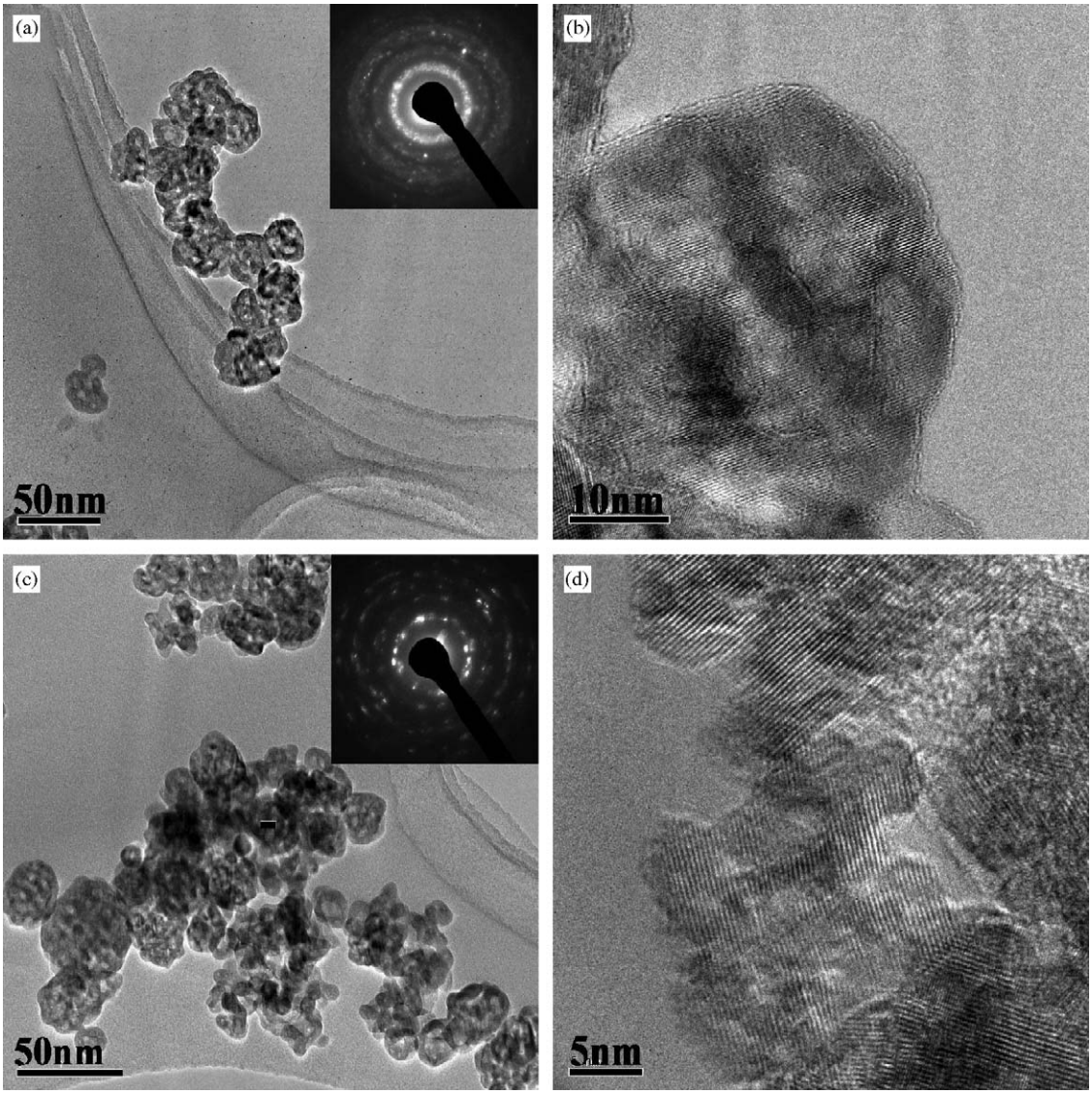

Fig. 5. HRTEM images of the 1 mol% cerium-doped TiO_2 nanoparticles: (a, b) as-synthesized; (c, d) calcined at 300 °C.

3.3. FTIR spectra

The FTIR spectra of the obtained samples calcined at 300 °C are shown in Fig. 6. For the 1, 5 mol% Ce-doped TiO_2 and undoped TiO_2, the peaks at 460, 620 and 910 cm^{-1} in the range of 400–1000 cm^{-1} are contribution from the anatase titania [11,20,24], which are also consistent with the observation from XRD and HRTEM. It is believed that the broad peaks at 3400 and 1638 cm^{-1} correspond to the surface-adsorbed water and hydroxyl groups [11,20]. The decrease in the intensities of these peaks in the FTIR spectra of the samples with increasing amount of doped cerium (Fig. 6b and c), implying that CeO_2 incorporation partly depletes the surface-adsorbed water and hydroxyl groups. The decrease of surface hydroxyl groups may be also beneficial for maintaining the mesostructures and preventing the sintering of nanoparticles upon following calcination. It is well known that the rapid condensation reactions between the large amounts of uncondensed Ti–OH, existed on the surface of the amorphous mesoporous TiO_2, would cause the walls of mesoporous TiO_2 to collapse during calcinations.

3.4. The N_2 adsorption–desorption experiment

Liquid nitrogen adsorption experimental results are presented in Table 1, the Brunauer–Emmett–Teller (BET) area of the sample was strongly dependent on the thermal treatment temperature and on cerium-doped amount. When the undoped TiO_2 sample was calcined at 500 °C, the surface area was measured as being equal to 232 $m^2 g^{-1}$, which corresponds to a decrease of 30% compared with the sample calcined at 300 °C. Whereas, 1 and 5 mol% Ce-doped samples treated at 300 °C present higher surface than undoped one. After calcination at 500 °C, their surface areas were measured as being equal to 273 and

289 $m^2 g^{-1}$, respectively. It corresponds to a decrease of 25% and 20% compared with 1 and 5 mol% Ce-doped samples calcined at 300 °C. These results confirm that the frameworks of cerium-doped mesoporous TiO_2 have relative higher thermal stabilities. This may be attributed to the presence of cerium oxide distributed on the TiO_2 matrix, which is in turn beneficial for effectively enhancing surface area of TiO_2 as reported in previous studies [27]. Larsson and Andersson also reported that the surface area of the TiO_2 support could also be stabilized by addition of CeO_2 to the CuO/TiO_2 system [33]. The surface areas and pore sizes of the obtained samples allow for comparison with previous results: Stone and Davis [12] (300 $m^2 g^{-1}$, 2.4 nm, calcined at 400 °C), Antonelli and Ying [41] (200 $m^2 g^{-1}$, 3.2 nm, calcined at 400 °C), Blanchard et al. [42] (350 $m^2 g^{-1}$, 2.1 nm, calcined at 350 °C).

The Barret–Joyner–Halenda (BJH) pore size distributions of the 1 mol% cerium-doped samples are shown in Fig. 7. The pore size distribution of the as-synthesized sample determined from desorption isotherm show a bimodal pore size distributions consist of smaller (1.9–3.2 nm) intra-particle pores and larger (12–62 nm) inter-particle pores. The narrower pore size distribution of the intra-particle pore size is in range of 1.9–3.2 nm centered at 2.3 nm, which is similar with the observation from HRTEM (Fig. 5). Moreover, the grain size becomes larger and mesopores begin to partly collapse upon calcination, which results in the intra-particle pore size shifting to a larger mesopore region. The sample calcined at 300 °C still maintains relatively narrow intra-particle pore size distribution. After calcination at 500 °C, the intra-particle pore distribution becomes weaken and broaden, which can be ascribed to the collapse of the intra-particle pores and the nanocrystallites growth of TiO_2. However, the pore size distribution of the inter-particle pores just changed slightly upon cacination, indicating that the inter-particles pores as well as the nanoparticle sizes changed insignificantly. As presented in Table 1, after calcinations at 800 °C, the two Ce-doped sample still maintains intra-particle mesopores, while this intra-particle mesopores disappeared for the undoped sample. These results show that the addition of cerium to the TiO_2 samples stabilizes their textural structure, hindering agglomeration and thus preventing mesopores from collapse. The dependence of

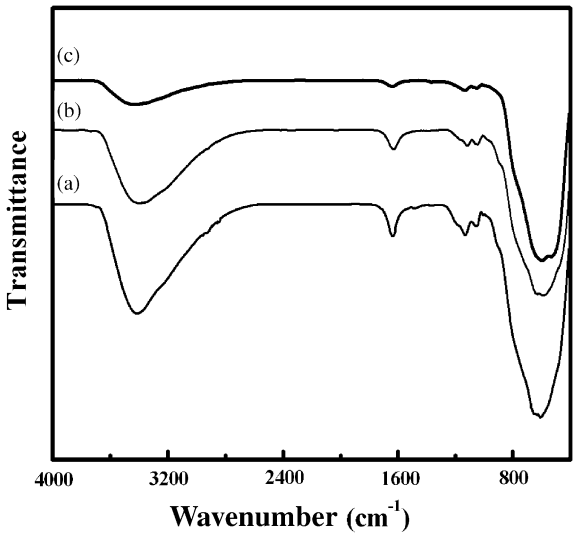

Fig. 6. FTIR spectra of samples calcined at 300 °C: (a) undoped, (b) 1 mol% cerium, and (c) 5 mol% cerium-doped samples.

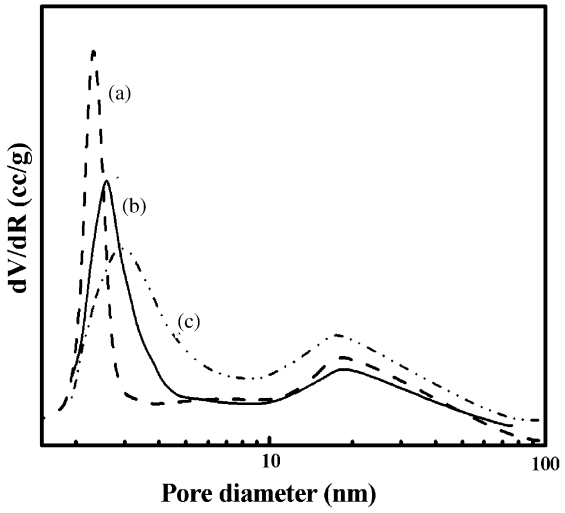

Fig. 7. Barret–Joyner–Halenda (BJH) pore size distribution plots of 1 mol% cerium-doped samples: (a) as-synthesized, and calcined, (b) 300 °C, (c) 500 °C.

Table 1
Summary of the properties of mesoporous cerium doped and undoped TiO_2 nanosized powders

Calcination temperatures (°C)	S_{BET}[a] ($m^2 g^{-1}$)			Mean pore size[b] (nm)			Total volume[c] ($cm^{-3} g^{-1}$)		
	5%	1%	Undoped	5%	1%	Undoped	5%	1%	Undoped
As-synthesized	465	454	438	2.3	2.3	2.1	0.59	0.58	0.56
300 °C	362	351	330	2.4	2.5	2.3	0.62	0.63	0.59
500 °C	289	273	232	2.7	2.9	2.5	0.56	0.57	0.53
800 °C	139	121	85	7.1	7.8	—	0.39	0.40	0.32

[a] S_{BET}—BET surface area calculated from the linear part of the BET plot.
[b] Mean pore size—estimated using the desorption branch of the isotherm.
[c] Total volume—single-point total pore volume of pores at $P/P_0 = 0.98$.

the pore size on the temperature of calcination is corroborated by the decrease of the BET surface area.

3.5. UV-Vis diffuse reflectance spectra (DRS)

UV-Vis DRS of the undoped, 1 and 5 mol% cerium-doped TiO_2 samples calcined at 300 °C are plotted in Fig. 8. The spectra shows that cerium incorporation to TiO_2 induces only a small red shift of the electronic absorption with respect to the undoped sample, and this red shift of the cerium-doped samples was found to increase with increasing in cerium content. The modification of the spectrum of Ce-doped TiO_2 with respect to undoped TiO_2 is consistent with the presence of a dispersed ceria component (in the form of very small crystallites) superimposed on the spectrum of the TiO_2 support [35].

3.6. Photocatalytic activity tests

The photocatalytic activities of the undoped and cerium-doped mesoporous TiO_2 nanopowders were detected by the degradation of RB under UV irradiation. For comparison, the photocatalytic activity of the commercial photocatalyst P25 was also measured under an identical condition. Photocatalytic tests were conducted in the dark confirmed that the measured phtotcatalytic activities are fully attributable to photo-induced processes. The results clearly demonstrate the superior performances of the obtained samples, as shown in Fig. 9. The degradation of RB is increased upon prolonging the irradiation time. As can be seen from the photocatalytic properties of 1 mol% Ce-doped samples calcined at different temperatures (Fig. 9A), the photocatalytic activity increased when the as-synthesized sample was calcined at 300 °C. While the photodegradation activity reduced when the calcination temperature is increased from 300 to 800 °C. This photocatalytic activity reduction may be attributed to the extensive decreases of specific surface area. Among the all samples tested, the optimum reactivity is observed for undoped mesoporous sample calcined at 300 °C, which causes 98% RB to be photodegraded after 120 min irradiation. And the photocatalytic degradation rate of cerium-doped samples decreased upon increasing cerium content (Fig. 9B). However, all of the doped and undoped samples calcined at 300 °C show better photoactivities than Deguess P25, although the maximum degradation rate corresponds to the undoped mesoporous anatase sample. These results suggest that the effect of cerium on the photoactivity of titania is different from the improvement of other rare-earth oxide like La and Eu on TiO_2 [27,28], which will be discussed preliminarily in the following section.

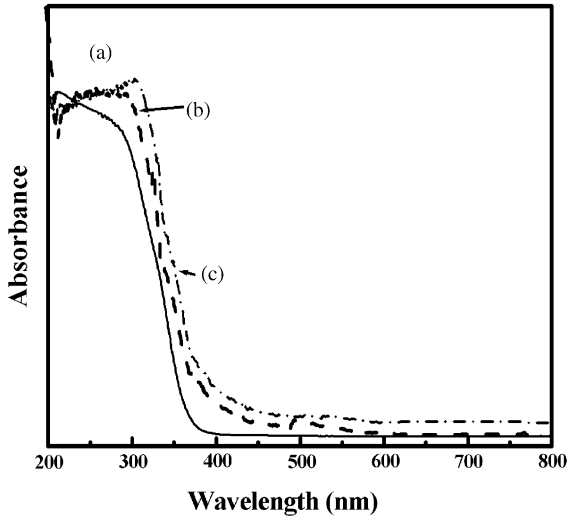

Fig. 8. UV-Vis diffuse reflectance spectra (DRS) of the samples calcined 300 °C: (a) undoped, (b) 1 mol% and (c) 5 mol% Ce-doped samples.

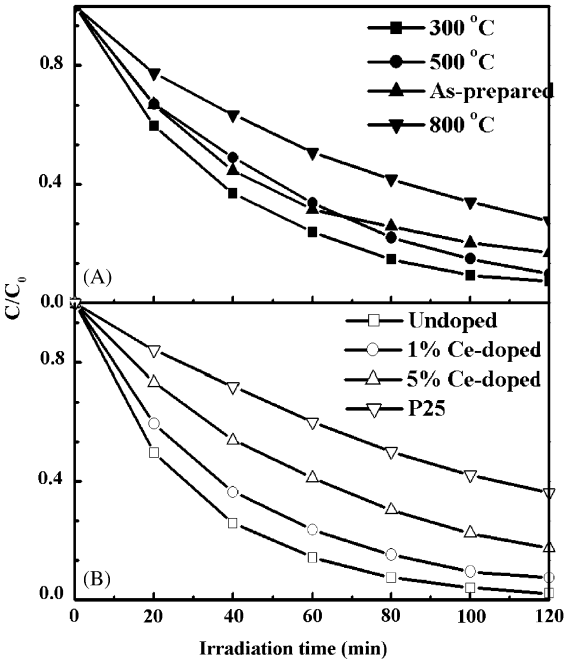

Fig. 9. (A): Photocatalytic properties of 1 mol% Ce-doped samples calcined at different temperatures, and (B) photocatalytic properties of the undoped, 1 and 5 mol% Ce-doped samples calcined at 300 °C as well as the P25 under UV-light radiation (RB, $c_0 = 1.0 \times 10^{-5}$ M, pH 6.0).

4. Discussion

4.1. Textural and phase transformation

It is known that the anatase-to-rutile transformation is related to many factors, such as impurities present in anatase, preparation conditions, precursors, dopants, morphologies of the particles, and others. LeDuc et al. [43] have reported that 5% La_2O_3-doped TiO_2 had long-term textural thermal stability up to 650 °C. Gopalan and Lin [44] also reported the evolution of pore structure and anatase phase stability up to 650 °C as a result of the addition of La_2O_3, and this is explained by possible

monolayer coverage of lanthana over TiO_2. Lin et al. [9,29] studied the influence of dopants in the anatase-to-rutile transformation temperature. In their work, XRD results of TiO_2 mixtures with 0.5 wt% rare-earth oxides revealed that these oxides can inhibit the phase transformation during the thermal treatment ($\leqslant 650\,^{\circ}C$ for TiO_2/La_2O_3, $\leqslant 700\,^{\circ}C$ for TiO_2/Y_2O_3 or CeO_2). Sibu et al. reported that the surface area of lanthanum doped TiO_2 nanocrystallite is increased by 25% compared to undoped one [27]. The rutile transformation temperature increased to 850 °C in the presence of CeO_2 from that of pure TiO_2 at 650 °C [27]. The inhibition of the phase transition was ascribed to the stabilization of the anatase phase by the surrounding rare-earth oxides through the formation of Ti–O–rare-earth element bonds [43–47]. At the interface, titanium atoms substituted the rare-earth elements in the lattice of the rare-earth oxides to form tetragonal Ti sites. The interaction between the different tetrahedral Ti atoms (in La_2O_3 and Y_2O_3) or between the tetrahedral Ti and octahedral Ti (in CeO_2) in the anatase is thought to retard the anatase-to-rutile transformation. Francisco and Mastelaro [34] also think that the likely formation of Ce–O–Ti interaction took place, inhibiting the transition of the anatase phase by observation of the XRD and Raman results of the $Ce_{0.09}Ti_{0.82}O_{1.91}Cu_{0.09}$ calcined at 650 °C. The Ce–O–Ti interaction blocks the Ti–O species at the interface with TiO_2 domains stabilizing them, inhibiting the agglomeration of TiO_2, and thus preventing the growth of titania nanocrystallite. On the other hand, according to Zhang and Banfield [46] though rutile is the most stable phase for a bulk material, when a large amount of surface is present (such as for nanoparticle smaller than 14 nm), anatase is stabilized, minimizing the total free energy of the system [46,47]. Moreover, Liao et al. have proved that the presence of interagglomerate pores can prevent the anatase grain growth [45].

In the present system, the diffraction peaks of the mesoporous Ce-doped samples change slowly upon calcination from 100 to 800 °C, indicating the anatase grains in the mesostructures have a relative high thermal stability, which is proposed to be due to segregation of the doped cations at the grain boundary. Moreover, the presence of crystallized mesoporous structure can also segregate and prevent the growth of anatase nanocrystallite in the nanoparticles. On the other hand, the decrease of crystallite sizes and the inhibition of titania phase transformation with the addition of cerium are consistent with the increase of surface area and the inhibition of the sintering of titania with adding cerium as observation from results and Table 1, which is consistent with previous results [34]. These results imply the addition of cerium to the titania modifies the mechanism of formation of the titania phases. Therefore, the thermal stabilities of anatase phase, nanocrystallite sizes, and the mesostructures can be attributed to the specific microstructures of our samples with cerium doping and large amount of mesopores existing between the nanocrystallite walls.

4.2. Photocatalytic activity

The mechanism of TiO_2 photocatalytic reactions has been the subject of extensive researches [9,27–29,48,49]. It is widely recognized that the surface-adsorbed water and hydroxyl groups can act as photoexcited hole traps on the catalyst surface and produce hydroxyl radicals, which are powerful oxidants in degrading organics [23]. The recombination of photogenerated carriers is the major factor to inhibit the reactivity of photocatalysts. The purpose of many research works is to decrease the recombination of photogenerated charge carriers, prolong the lifetime of the carriers, and improve the separation efficiency of photogenerated charge carriers. On the other hand, the organic material should be preconcentrated at the semiconductor surface in order to effectively trap the respective reactive radicals. Generally, stable mesostructures allow rapid diffusion of various reactants and products during photocatalytic reaction and enhance the speed of photocatalytic reactions, and also can offer more active sites to adsorb water and hydroxyl groups. Sibu et al. [27] reported that the surface area of lanthanum-doped TiO_2 nanocrystallite is increased by 25% compared to undoped one, and the lanthanum-doped TiO_2 can provide more adsorption sites in doped samples, making them more efficient catalysts. The enhanced photoactivity of TiO_2 doped by rare-earth oxide such as europium, praseodymium, and ytterbium oxides, was recently reported by Ranjit et al. [28]. The high activity of rare-earth oxide/TiO_2 photocatalyst is attributed to the enhanced electron density imparted to the TiO_2 surface by the dopants.

On those rare-earth ion doping, the Ti^{4+} at the interface substitute for the lanthanum in the lattice of lanthana to form tetrahedral Ti sites. This substitute not only inhibits the phase transformation to rutile, but also creates a charge imbalance. The charge imbalance must be satiated, therefore, more hydroxide ions would be adsorbed on the surface. The hydroxide ions acts as hole traps that prevent electrons–holes recombination and thus creates a higher quantum yield. The traps have been observed in TiO_2 by several groups [48] and are assigned to coordinatively unsaturated titanium ions at the surface of the TiO_2 crystals. In the present system, the clear enhancement of degradation rate of undoped and cerium-doped mesoporous anatase nanoparticle samples, compared with that of P25, is probably contributed by coexisting of larger surface areas and smaller crystallite size, which can supply a great number of the surface states available to adsorb hydroxide and combine with RB. In general, smaller crystalline size means more powerful redox ability due to the quantum-size effect [3,23,26]. While crystallized mesoporous frameworks in the obtained nanoparticles not only increased the surface areas which is beneficial for transportation and exchanges of organic and productions, but also the smaller crystallite size is in favor of the separation of the photogenerated carriers, prolong the lifetime of the

carriers, and then improve the photocatalytic activity of the mesoporous nanoparticles compared with P25.

By examining the photocatalytic activity changes at different temperatures, it can be found that the photocatalytic activity increased when the calcination temperature is increased to 300 °C. Compared with the as-synthesized sample, the sample calcined at 300 °C possesses reduced surface area but a more excellent crystallinity, as indicated in Fig. 3 and Table 1. Therefore, we think that the degree of crystallinity also played a major role in the photoactivity of TiO_2. Previous researchers showed that polycrystalline samples of TiO_2 have high photoproduction rates of dihydrogen as compared with amorphous forms [49]. Ohtani et al. determined that the photocatalytic activity of TiO_2 with a constant particle size increased linearly with the fractional crystallinity of anatase [18]. The photodegradation activity reduced when the calcination temperature is increased from 300 to 800 °C. This photocatalytic activity reduction may be attributed to the extensive decreases of specific surface area.

Our experimental results also indicated the lower photocatalytic activities of cerium-doped samples than undoped one. It is known that the photogenerated $OH^{\bullet}$ radicals drive degradation reactions, which can eventually lead to the decomposition of organic pollutants. The Ti^{4+}–$OH^{\bullet}$ entities are formed by a surface hydroxyl trapping a hole. However, Coronade et al. [35] have found that some of the photoproduced holes are stabilized as Ti^{4+}–O^{-} radicals in the CeO_2/TiO_2 catalyst. The CeO_2/TiO_2 catalyst displays a reduced concentration of Ti^{4+}–O^{-} radicals, which is apparently less prone to trap photogenerated holes than the undoped TiO_2. In addition, the coverage of the TiO_2 surface by ceria entities removes $OH^{\bullet}$ groups, which will lead to decrease not only the active $OH^{\bullet}$ radicals but also the adsorption sites for organic pollutants [50]. Therefore, they thought that the lower photocatalytic rate of CeO_2/TiO_2 is very likely due to the partial blockage by ceria of the surface centers, which may be lead to decrease the trapping efficiency of the holes and the adsorption of the organic. Also, Lin et al. [9,29] reported the mixtures of titania with Y_2O_3 or La_2O_3 were shown to have higher photocatalytic activities than pure TiO_2, while the mixture of TiO_2 with CeO_2 have lower photoactivity than pure TiO_2. They ascribed the lower photocatalytic activities of the mixture of TiO_2 and CeO_2 to the change in the amount of surface hydroxyl groups resulting from the interaction between the rare-earth oxides and TiO_2.

Considering above discussion, we can draw following conclusions. Firstly, the lower photocatalytic activities of cerium-doped samples than undoped one is probably contributed by the partial blockage of the surface sites available for RB. Because the photocatalytic activities of catalysts can ascribe to the equilibrium of the number of surface hydroxyl and the amount of adsorbed RB on the surface of mesoporous TiO_2 nanoparticles. The number of surface hydroxyl groups was less due to the blockage of cerium on the titania, but the amount of adsorption of RB on cerium-doped TiO_2 surface was higher because doped titania has higher surface areas. The FTIR spectra of samples also show that the surface hydroxyl of 1 and 5 mol% cerium-doped samples were less than that of undoped one, although they have larger surface areas (Table 1). Secondly, the higher activities at 1 mol% cerium-doped sample, compared with 5 mol% cerium-doped sample calcined at 300 °C, may be due to the fact that there is an optimal doping concentration of cerium ions in TiO_2 for the most efficient separation of photogenerated carriers. Pleskov [51] reported that there is an optimal concentration of dopant ions to make the thickness of space charge layer substantially equal to the light penetration depth, because the space charge region becomes very narrow when the concentration of doping ions is too high, and the penetration depth of light into TiO_2 greatly exceeds the space charge layer, which will result in the recombination of the photogenerated carriers becoming easier. Finally, the enhancement of the photon harvesting efficiency derived from the red shift of the electronic absorption of cerium-doped TiO_2, is not significant under these conditions, because the energy of most of the photons emitted by the UV source (maximum emission at 365 nm) is larger than the band gap interval of the studied materials. Further studies are necessary to clarify the effects of the surface area, doping, microstructure, and crystalline composition of TiO_2 on the photocatalytic activity.

5. Conclusions

Mesoporous cerium-doped TiO_2 nanosized powders with high surface area and stable anatase wall were prepared by using CTAB as directing and pore-forming agent via hydrothermal process. The textural and phase transformation of titania have been studied with the objective to better understand the effect of the addition of cerium dopants. It has been found that the addition of cerium to the TiO_2 system increased surface area of mesoporous TiO_2 nanoparticles and prevented the sintering of samples calcined at higher temperature. And then, this prevented mesopore collpase and the anatase-to-rutile phase transformation. The obtained mesoporous undoped, cerium-doped nanoparticles are shown to exhibit higher photocatalytic activity than photocatalyst P25, but the maximum degradation rate corresponds to the undoped mesoporous nanoparticles. The negative effect of cerium incorporation to the titania samples on the photocatalytic performance may be ascribed to the partial blockage of the surface sites available for RB photodegradation.

Acknowledgment

Dr. T.Y. Peng acknowledges the Natural Science Fund of China (20573078), the Natural Science Fund of Hubei Province, China (2004ABA083), and the Project sponsored by SRF for ROCS, SEM, China. Authors are indebted to

Dr. Wang from Center for Electron Microscopy of Wuhan University, for the HRTEM images.

References

[1] P.W. Morrison, R. Raghavan Jr., A.J. Timpone, C.P. Artelt, S.E. Pratsinis, Chem. Mater. 9 (1997) 2702–2708.
[2] Y. Murakami, T. Matsumoto, Y. Takasu, J. Phys. Chem. B 103 (1999) 1836–1840.
[3] M.R. Hoffmann, S.T. Martin, W. Choi, D.W. Bahnemann, Chem. Rev. 95 (1995) 69–96.
[4] Y.T. Kwon, K.Y. Song, W.I. Lee, G.J. Choi, Y.R. Do, J. Catal. 191 (2000) 192–199.
[5] A.J. Maira, K.L. Yeung, C.Y. Lee, P.L. Yue, C.K. Chan, J. Catal. 192 (2000) 185–196.
[6] A.J. Maira, K.L. Yeung, J. Soria, J.M. Coronado, C. Belver, C.Y. Lee, V. Augugliario, Appl. Catal. B 29 (2001) 327–336.
[7] X. Fu, W.A. Zeltner, M. Anderson, Appl. Catal. B 6 (1995) 209–224.
[8] A. Linsebigler, G. Lu, J.T. Yates, Chem. Rev. 95 (1995) 735–758.
[9] J. Lin, J.C. Yu, D. Lo, S.K. Lam, J. Catal. 183 (1999) 368–372.
[10] M. Anpo, Stud. Surf. Sci. Catal. 130 (2000) 157–163.
[11] G. Soler-Illia, A. Louis, C. Sanchez, Chem. Mater. 14 (2002) 750–759.
[12] V.F. Stone Jr., R.J. Davis, Chem. Mater. 10 (1998) 1468–1474.
[13] T.Y. Peng, A. Hasegawa, J.R. Qiu, K. Hirao, Chem. Mater. 15 (2003) 2011–2016.
[14] P. Yang, D. Zhao, D.I. Margolese, B.F. Chmelka, G.D. Stucky, Nature 396 (1998) 152–155.
[15] (a) C. Wang, Q. Li, R.D. Wang, Mater. Lett. 58 (2004) 1424–1426; (b) J.Y. Zheng, J.B. Pang, K.Y. Qiu, Y. Wei, J. Mater. Chem. 11 (2001) 3367–3372.
[16] C.C. Wang, J.Y. Ying, Chem. Mater. 11 (1999) 3113–3120.
[17] C.N. Rusu, J.T. Yates, Langmuir 13 (1997) 4311–4316.
[18] B. Ohtani, Y. Ogawa, S.I. Nishimoto, J. Phys. Chem. B 101 (1997) 3746–3752.
[19] S.H. Elder, Y. Gao, X. Li, J. Liu, D.E. McCready, C.F. Windisch, Chem. Mater. 10 (1998) 3140–3145.
[20] J.C. Yu, L.Z. Zhang, Z. Zheng, J.C. Zhao, Chem. Mater. 15 (2003) 2280–2288.
[21] Y.D. Wang, C.L. Ma, X.D. Sun, H.D. Li, Mater. Lett. 54 (2002) 359–363.
[22] V. Augugliaro, S. Coluccia, V. Loddo, L. Marchese, G. Martra, L. Palmisano, M. Schiavello, Appl. Catal. B 20 (1999) 15–27.
[23] J.C. Yu, L.Z. Zhang, J.G. Yu, Chem. Mater. 14 (2002) 4647–4653.
[24] K.E. Karakitsou, X.E. Verykios, J. Phys. Chem. 97 (1993) 1184–1189.
[25] W. Choi, A. Termin, V. Hoffmann, Angew. Chem. Int. Ed. Engl. 33 (1994) 1091–1092.
[26] T. Lopez, J. Hernandez-Ventura, R. Gomez, F. Tzompantzi, E. Sanchez, X. Bokhimi, A. Garcya, J. Mol. Catal. A: Chem. 167 (2001) 101–107.
[27] C.P. Sibu, S. Rajesh Kumar, P. Mukundan, K.G.K. Warrier, Chem. Mater. 14 (2002) 2876–2881.
[28] (a) K.T. Ranjit, E. Joselevich, I. Willner, J. Photochem. Photobiol. A: Chem. 96 (1996) 185–192; (b) K.T. Ranjit, H. Cohen, I. Willner, S. Bossmann, A. Braun, J. Mater. Sci. 34 (1999) 5273–5280; (c) K.T. Ranjit, I. Willner, S.H. Bossmann, A.M. Braun, Environ. Sci. Technol. 35 (2001) 1544–1549.
[29] J. Lin, J.C. Yu, J. Photochem. Photobiol. A: Chem. 116 (1998) 63–67.
[30] K.L. Frindell, M.H. Bartl, M.R. Robinson, G.C. Bazan, A. Popitsch, G.D. Stucky, J. Solid State Chem. 172 (2003) 81–88.
[31] W.Z. Zhang, T.J. Pinnavaia, Chem. Commun. (1998) 1185–1186.
[32] A. Trovarelli, Catal. Rev. Sci. Eng. 38 (1996) 439–520.
[33] P.O. Larsson, A. Andersson, J. Catal. 179 (1998) 72–89.
[34] M.S.P. Francisco, V.R. Mastelaro, Chem. Mater. 14 (2002) 2514–2518.
[35] J.M. Coronado, A.J. Maira, A. Martinez-Arias, J.C. Conesa, J. Soria, J. Photochem. Photobiol. 150 (2002) 213–221.
[36] A.W. Xu, Y. Gao, H.Q. Liu, J. Catal. 207 (2002) 151–157.
[37] T.Y. Peng, D. Zhao, H.B. Song, C.H. Yan, J. Phys. Chem. B 109 (2005) 4947–4952.
[38] T.Y. Peng, D. Zhao, H.B. Song, C.H. Yan, J. Mol. Catal. A: Chem. 238 (2005) 119–126.
[39] Y. Yue, Z. Gao, Chem. Commun. 18 (2000) 1755–1756.
[40] S. Cabrera, J. El-Haskouri, A. Beltran-Portier, D. Beltran-Portier, M.D. Marcos, P. Amoros, Solid State Sci. 2 (2002) 513–518.
[41] D.M. Antonelli, Y.J. Ying, Angew. Chem. Int. Ed. Eng. 34 (1995) 2014–2017.
[42] J. Blanchard, F. Schuth, P. Trens, M. Hudson, Microporous Mesoporous Mater. 39 (2000) 163–170.
[43] C.A. LeDuc, J.M. Campbell, J.A. Rossin, Ind. Eng. Chem. Res. 35 (1996) 2473–2476.
[44] R. Gopalan, Y.S. Lin, Ind. Eng. Chem. Res. 34 (1995) 1189–1195.
[45] S.L. Liao, K.D. Pae, W.E. Mayo, Nanostruct. Mater. 3 (1995) 319–325.
[46] H. Zhang, J.F. Banfield, J. Mater. Chem. 8 (1998) 2073–2076.
[47] E.L. Crepaldi, G.J. de A.A. Soler-Illia, D. Grosso, F. Cagnol, F. Ribot, C. Sanchez, J. Am. Chem. Soc. 125 (2003) 9770–9786.
[48] T. Nakahira, M. Gratzel, J. Phys. Chem. 88 (1984) 4006–4010.
[49] R.S. Davidson, C.L. Morrison, J. Abraham, J. Photochem. 24 (1994) 27–31.
[50] A.J. Maira, J.M. Coronado, V. Augugliario, K.L. Yeung, J.C. Conesa, J. Soria, J. Catal. 202 (2001) 413–420.
[51] Y.V. Pleskov, Sov. Electrochem. 17 (1981) 1–6.